Drying curve simulation and LF-NMR online monitor of water state in ursolic acid loaded chitosan nanoparticles during microwave freeze drying

Xing Ren, Xu Duan*, Weiwei Cao, Lujie Zhao, Guangyue Ren, Panpan Liu

(*College of Food and Bioengineering, Henan University of Science and Technology, Luoyang 471023, Henan, China*)

Abstract: The changes in various states of water in ursolic acid (UA) loaded chitosan nanoparticles were assessed using low-field nuclear magnetic resonance (LF-NMR) during microwave freeze drying (MFD) process, and six thin-layer models were applied to simulate the drying kinetics. UA nanoparticles were dried at different microwave power densities (1 W/g, 2 W/g and 4 W/g). The results showed that three water fractions with different transverse relaxation times (T_2) were detected in fresh UA nanoparticles. The T_2 relaxation time of water decreased significantly with drying time at different microwave power densities. And the mutual migration and transformation of water in different states during the drying process of chitosan nanoparticles occurred. Furthermore, mathematical model analysis showed that the Page model provided the best description during the process of UA nanoparticle dried by MFD. The Page model can better simulate the drying kinetics of chitosan nanoparticles dried by MFD, and LF-NMR technology can monitor the changes in water status of UA nanoparticles. The results revealed that LF-NMR can monitor the changes of water in UA nanoparticles during the drying process.

Keywords: microwave, drying, chitosan nanoparticles, water distribution

DOI: 10.25165/j.ijabe.20231604.7519

Citation: Ren X, Duan X, Cao W W, Zhao L J, Ren G Y, Liu P P. Drying curve simulation and LF-NMR online monitor of water state in ursolic acid loaded chitosan nanoparticles during microwave freeze drying. Int J Agric & Biol Eng, 2023; 16(4): 263–268.

1 Introduction

Ursolic acid (UA) is a representative pentacyclic triterpenoid carboxylic acid existing in many medicinal plants[1]. UA has multiple pharmacological effects such as anti-inflammatory, antibacterial, antitumor, antioxidant activity[2]. Although UA has various functional properties, it has poor solubility and low bioavailability[3], which limits their use in functional foods. To improve the solubility and bioavailability of UA, UA loaded chitosan nanoparticles were prepared using the cross-linking agent sodium tripolyphosphate by ionotropic gelation method. Drying is an essential step to obtain and preserve UA nanoparticles. Therefore, it is of importance to achieve high-efficiency control of water content of the microcapsules via evaluating dry characteristics of UA nanoparticles.

In recent years, microwave freeze drying (MFD), as a new type of drying technology, has been extensively studied due to its advantages in improving food quality and reducing energy consumption[4]. Freeze drying (FD) as a common freeze drying method also can obtain dried product in high quality, but it always requires more time and energy consumption. For example, freeze dried Litsea cubeba essential oil microcapsules required 48 h[5]. The pumpkin seed oil microcapsules were dried for 48 h using freeze drier[6]. Compared with FD, MFD can greatly improve drying rate, reduce the drying time[7]. In order to avoid the disadvantages of FD, MFD can be used to produce products in high quality with less energy consumption. Duan et al.[8] reported that the time for drying sea cucumber by MFD was nearly a half of that for FD, and there were no significant differences on the quality of microwave freeze- and freeze dried sea cucumber. Jiang et al.[9] reported that compared with FD, MFD can reduce drying time by 40% and provide similar quality. Moreover, MFD could realize better dry mushroom quality and drying efficiency than FD[10]. Therefore, MFD is one of the most promising technologies for accelerating drying and improving the overall quality of products[11]. To effectively improve the quality of MFD products and optimize the drying process, it is necessary to use mathematical models to describe the drying process under different drying conditions. Thin layer drying equations are of importance in the mathematical modeling in the drying process, which can better understand the drying mechanism, effectively map the trend of drying characteristics, and optimize energy efficiency[12,13]. Li et al.[14] found that the *Page* model could provide suitable description on the foam mat drying process of cantaloupe puree. Parveen et al.[15] predicted the drying kinetic of aonla varieties through the application of the *Newton* model. Kadriye et al.[16] found that the Two-term exponential model could adequately describe the drying behavior of kiwi slices. However, information on the study of the drying kinetic model and drying mathematical models of UA nanoparticles dried by MFD is still unknown.

Knowledge of water state change of materials during drying is important for prediction of dehydration. Low field nuclear magnetic resonance (LF-NMR), an excellent noninvasive tool, is an advantageous choice for analyzing dynamic water states of product during drying with high sensitivity and short detection time[17]. The change in relaxation time in LF-NMR was used to explain the water mobility and distribution inside the sample from a microscopic

Received date: 2022-03-15 **Accepted date:** 2023-06-22

Biographies: **Xing Ren**, MS, research interest: food engineering, Email: rennxing@163.com; **Weiwei Cao**, PhD, Associate Professor, research interest: food science and engineering, Email: caoweiwei@haust.edu.cn; **Lujie Zhao**, MS, research interest: food science and engineering, Email: ZLujie942658@163.com; **Guangyue Ren**, PhD, Professor, research interest: drying technology of agricultural products, Email: guangyueyao@163.com; **Panpan Liu**, MS, research interest: food science and engineering, Email: liupanpan1002@163.com.

***Corresponding author: Xu Duan**, PhD, Professor, research interest: theory research on drying technology of agricultural products. Food and Biology Engineering College, Henan University of Science & Technology, Luoyang, Henan 471023, China. Tel: +86 -13653872870, Email: duanxu_dx@163.com.

point of view. The ^{1}H proton relaxation time was measured to obtain the moisture information about free water, immobile water and bound water in materials. LF-NMR is widely used in food drying process to analyze changes in water distribution and mobility[18]. Li et al.[19] adopted LF-NMR to monitor the water state and distribution of mulberries in real-time during the drying process and the T_2 reduction trend of free water was consistent with the drying kinetic curves. Lin et al.[20] studied that the water mobility and distribution of soybean antioxidant peptide powders were monitored in real-time using LF-NMR during storage environment. Xu et al.[21] reported that LF-NMR could be used to understand the water changes of the broccoli samples during the drying process by studying the water distribution. LF-NMR technique is preponderantly used in evaluating the effect of pullulan on the water distribution of rice starch gels[22]. Therefore, LF-NMR can effectively monitor changes in the water state of material during drying. The water state and distribution of microwave freeze-dried UA loaded chitosan nanoparticles measured using LF-NMR may be more effective and intuitive. However, researches on evaluating drying characteristics of UA nanoparticles via LF-NMR cannot be available.

In this study, UA loaded chitosan nanoparticles were dried by MFD at different microwave power levels, and mathematical models were used to reveal the dehydration of UA nanoparticles dried by MFD. Meanwhile, the drying curve and LF-NMR technique were chosen to explore the water migration characteristics of UA loaded chitosan nanoparticles.

2 Materials and methods

2.1 Materials

Chitosan (degree of deacetylation ≥ 90.0%), with a molecular weight of 30,000, was purchased from Shanghai Lanji Technology Development Co., Ltd. (Shanghai, China). UA (purity: 98%) was purchased from Chengdu Biopurify Phytochemicals Ltd. (Chengdu, Sichuan, China). Sodium tripolyphosphate (TPP) and Tween-80 were analytical grade reagents purchased from Tianjin Deen Chemical Reagent Co., Ltd. (Tianjin, China). The remained chemical reagents were of analytical grade.

2.2 Preparation of UA loaded chitosan nanoparticles

UA loaded chitosan nanoparticles were prepared according to the method of Yan et al.[23] with some modification. Chitosan was added to 1% (w/v) acetic acid solution for magnetic stirring for 8 h at 25ºC to obtain transparent solution. The pH of chitosan solution was adjusted to 5.0 with 0.1 g/mL sodium hydroxide solution, and then 1% Tween-80 was added and magnetically stirred for 20 min at 25ºC. The UA solution dissolved in ethanol was further added to the above solution at the UA-chitosan mass ratio of 4:1, and under magnetic stirring for 30 min. TPP solution of 2.0 mg/mL was slowly dropped into the mixed solution at the chitosan-TPP mass ratio of 4:1, and magnetically stirred for 45 min to obtain UA loaded chitosan nanoparticles suspension. The nanoparticles suspension was centrifuged at 12 000 r/min for 20 min, and the precipitate was washed with distilled water to remove unbound UA, and dried for further studies.

2.3 Drying experiments

The precipitate of the same weight is filled in a 60 mm petri dish and dried by a microwave freeze dryer which was developed by Duan et al.[24] The precipitate was frozen at –25ºC for at least 8 h. The pressure of the independent polypropylene drying cavity and cold trap temperature were carried out at 100 Pa and –40ºC, respectively. The power density loading levels of microwave were set at 1.0 W/g, 2.0 W/g and 4.0 W/g, respectively. Remove the petri dishes every 15 min and weigh them, put the samples into NMR bottles, and then put the new petri dishes containing the sample into it to dry. All the above drying experiments were performed in triplicate.

2.4 Detection of LF-NMR

The relaxation time (T_2) of UA loaded chitosan nanoparticles was measured by an LF-NMR analyzer (Shanghai Nguyen Electronic Technology Co., Ltd.) with a Carr-Purcell-Meiboom-Gill (CPMG) pulse sequence. Take 5 mg of UA nanoparticles each time with forceps and place them in a NMR bottle. The main LF-NMR parameters were set as follows: main frequency (SF), 21 MHz; sampling point (TD), 89 998; offset frequency (O1), 306 350.93; sampling frequency (SW), 100 kHz; time echo (TE), 0.4 ms; time waiting (TW), 1500 ms; the number of scan (NS), 16 and the number of echoes (NECH), 2250. The T_2 inversion program was used to obtain the relaxation map of the samples.

2.5 Mathematical modeling of drying curves

2.5.1 Moisture content and moisture ratio (MR)

The moisture content in UA loaded chitosan nanoparticles was determined using an oven at 105ºC by direct drying method[25]. All the tests were performed in triplicate. During the MFD experiments, the moisture content, drying rate (DR) and moisture ratio (MR) were calculated using Equations (1)-(3), respectively.

$$W_t=\frac{m_t-m_g}{m_t}\times 100 \tag{1}$$

$$DR=\frac{M_{t+dt}-M_t}{dt} \tag{2}$$

$$MR=\frac{X_t-X_e}{X_o-X_e}\approx\frac{X_t}{X_o} \tag{3}$$

where, W_t and MR are the wet basis moisture content (%) and the moisture ratio of the samples, respectively; DR is the drying rate, %/min; m_t is the weight at any time, g; m_g is the constant weight after drying at 105ºC, g; M_{t+dt} is moisture content at the time of t+dt, %; t is the time interval of drying, s; X_t is the moisture content of the chitosan nanoparticles, %; X_o is the initial moisture content (%) and X_e is equilibrium moisture content (%) of the samples, which is usually ignored in engineering applications[26].

2.5.2 Mathematical models

Six mathematical models (Table 1) were selected for describing the MFD process of UA loaded chitosan nanoparticles[27,28]. The fitness between the mathematical model and the experimental data could be evaluated by the highest value of the coefficient of determination (R^2) and the lowest values of the chi-square test (χ^2) and the root mean square error (RMSE) [29]. The R^2, χ^2 and RMSE values were calculated with the following Equations (4)-(6) [30].

$$R^2=1-\frac{\sum_{i=1}^{N}\left(MR_{exp,i}-MR_{pre,i}\right)^2}{\sum_{i=1}^{N}\left(\overline{MR}_{exp}-MR_{exp,i}\right)^2} \tag{4}$$

$$\chi^2=\frac{\sum_{i=1}^{N}\left(MR_{exp,i}-MR_{pre,i}\right)^2}{n-z} \tag{5}$$

$$\mathrm{RMSE}=\left[\frac{1}{N}\sum_{i=1}^{N}(MR_{pre,i}-MR_{exp,i})^2\right]^{\frac{1}{2}} \tag{6}$$

where, $MR_{exp,i}$, $MR_{pre,i}$, n and z are the experimental moisture ratios,

the predicted moisture ratio, the number of observations and a constant, respectively.

Table 1 Mathematical models tested for simulating drying curves

Model	Mathematical equation
Newton	MR=exp(-kt)
Page	MR=exp(-kt^n)
Hendersnn-Pahis	MR= a exp(-kt)
Cubic	MR= a+bt+ct^2+dt^3
Diffusion approach	MR=a exp(-kt)+(1-a)exp(-kbt)
Two-term exponential	MR=a exp(-kt)+(1-a)exp(-kat)

2.6 Statistical analysis

Results were performed as means ± standard deviation. Origin 2017 software was used to draw result diagrams. SPSS software (version 25, SPSS Inc., Chicago, IL) was used to analyze the significance of the data. In order to determine the significant difference between the group samples, the confidence interval was selected as 95% (p<0.05).

3 Results and discussion

3.1 Drying characteristics

UA-loaded chitosan nanoparticles were dehydrated at three microwave power density of 1, 2 and 4 W/g to equilibrium moisture content. The drying curve and drying rate curves of UA-loaded chitosan nanoparticles are shown in Figure 1. Figures 1a and 1b show that during the MFD process, the drying curves displayed similar trend, but the greater the microwave power density, the shorter the drying time and the greater the maximum drying rate. Figure 1a showed that at microwave power density level of 1, 2 and 4 W/g, the time to reach the final moisture content were 150 min, 120 min and 110 min, respectively. The drying time decreased with the increase of microwave power density, similar results were also found in drying Chinese Yam (Dioscorea opposite) Tubers by MFD[31]. Compared with the drying time at 1 W/g, the drying time at 2 and 4 W/g were reduced by 20% and 26.7%, respectively. This might be attributed to that the higher microwave power density provided more energy for water molecules to evaporate. It can be seen from Figure 1b that the drying rate is mainly manifested as a deceleration stage in the whole process. When the microwave power density is 4 W/g, the maximum drying rate can reach 1.87 %/min, while the drying rate at 1 W/g is the smallest, and the maximum value at 1 W/g can reach 1.07 %/min. The reason may be that when the microwave power density is higher, the penetration effect of the microwave radiation energy is stronger, and the drying rate is also higher. Therefore, in the actual drying process, the microwave power density can be appropriately enhanced to increase the drying rate to efficiently obtain chitosan nanoparticles.

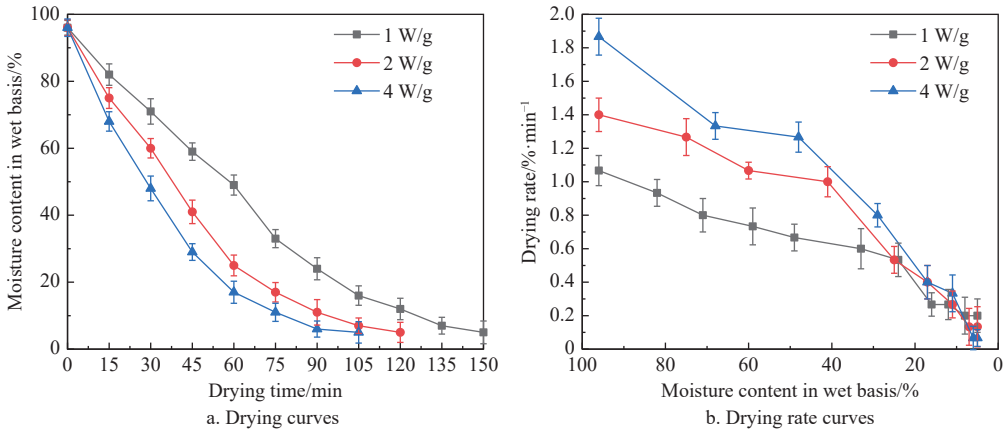

Figure 1 Drying curves and drying rate curves of UA loaded chitosan nanoparticles at different microwave power densities

3.2 Models of drying kinetics

The data obtained during the drying process of UA nanoparticles at different microwave power densities were fitted to six mathematical models, as listed in Table 2. The constants of the drying model varied with the microwave power densities. The higher value of R^2 and the lower values of the χ^2 and RMSE indicated accuracy of mathematical tested models to describe the drying behavior. Table 2 shows that the values of R^2 are greater than 0.99 and the χ^2 and RMSE values are both less than 0.01, indicating that all six excellent models have a good fit. Among them, the highest R^2 value given by the Page model was 0.999 91, and the lowest χ^2 and RMSE values were 8.9×10^{-6} and 0.002 829, respectively. More specifically, R^2 value obtained by the *Page* model fitting at different microwave power densities was ordered 4 W/g > 2 W/g > 1 W/g. Therefore, the *Page* model was selected to describe the drying kinetics of UA-loaded chitosan nanoparticles. This was also in agreement with that the *Page* model was the most suitable model to exhibit the drying characteristics of ripe mango cubes[32]. Herein, the constants obtained in the *Page* model can be better used to fit the drying processes of UA-loaded chitosan nanoparticles.

3.3 Drying mathematical model verification

To verify the accuracy of the *Page* model, the results of the experimental values and the predicted values of *MR* under 1, 2, and 4 W/g conditions were compared in Figure 2. It can be seen from Figure 2 that the *Page* model curve was basically consistent with the experimental value. At the same time, Figure 3 shows that the experimental values are equal to the predicted values of *MR*. Moreover, Figure 3 shows that the experimental value and the predicted value have a high degree of fit, and the Pearson correlation coefficient is 0.997, indicating that the Page model could better reflect *MR* in MFD of UA-loaded chitosan nanoparticles.

3.4 Water states in wet chitosan nanoparticles evaluated by LF-NMR

The indicator of water mobility T_2 is generally used to measure the binding force of water and matter in materials. The larger the T_2 is, the weaker the water and matter is bound[33]. Figure 4 shows that the water states in wet chitosan nanoparticles. The internal moisture in chitosan nanoparticles can be divided into three areas, and the bound water range is 0.1-10 ms (T_{21}), the immobile water range is 10-100 ms (T_{22}) and the free water range is 100-1000 ms (T_{23})[34]. The peak area can characterize the moisture content, and the

Table 2 Statistical analyses for different microwave power density for drying processes of UA-loaded chitosan nanoparticles

Model	Microwave power density/W·g^{-1}	R^2	χ^2	RMSE
Newton	1	0.990 32	0.000 834	0.028 879
	2	0.996 38	0.000 382	0.019 557
	4	0.998 46	0.000 185	0.013 627
	average	0.995 05	0.000 467	0.020 688
Page	1	0.999 84	0.000 013 7	0.003 702
	2	0.999 91	0.000 010 8	0.003 298
	4	0.999 98	0.000 002 2	0.001 488
	average	0.999 91	0.000 008 9	0.002 829
Hendersnn-Pahis	1	0.989 26	0.000 925	0.030 422
	2	0.995 87	0.000 437	0.020 907
	4	0.998 20	0.000 216	0.014 719
	average	0.994 44	0.000 526	0.022 016
Cubic	1	0.873 43	0.003 702	0.124 819
	2	0.895 93	0.017 620	0.132 747
	4	0.911 24	0.018 640	0.136 519
	average	0.893 53	0.013 320 7	0.131 362
Diffusion approach	1	0.998 98	0.000 122	0.009 451
	2	0.995 18	0.000 510	0.022 583
	4	0.984 00	0.001 920	0.043 817
	average	0.992 72	0.000 850	0.025 284
Two-term exponential	1	0.992 99	0.000 604	0.024 585
	2	0.997 46	0.000 307	0.017 525
	4	0.998 64	0.000 163	0.012 771
	average	0.996 36	0.000 358	0.018 294

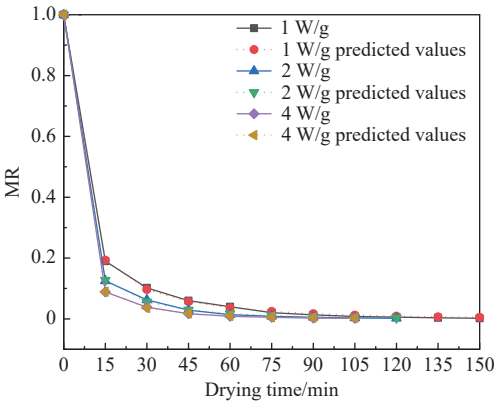

Figure 2 Predicted values versus experimental values of MR at different microwave power densities

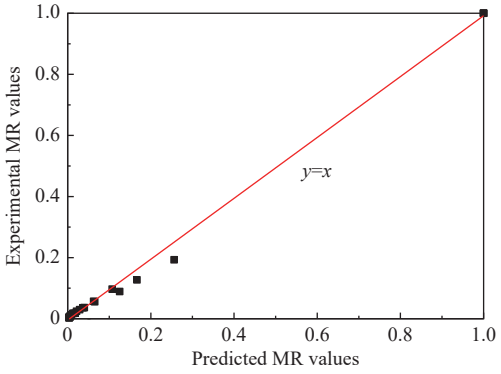

Figure 3 Fitting curve of drying mathematical model

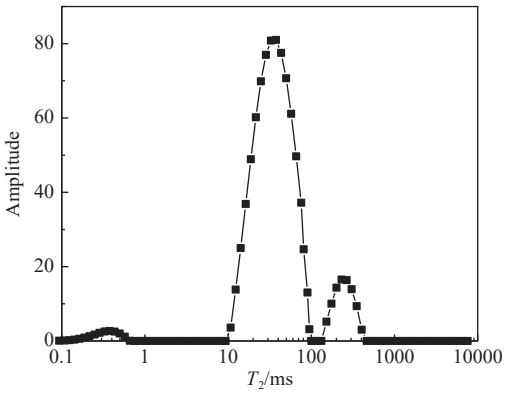

Figure 4 Water states in wet chitosan nanoparticles evaluated by LF-NMR

corresponding peak areas of T_{21}, T_{22} and T_{23} are A_{21}, A_{22} and A_{23}, respectively, which represent the content of bound water, immobile water and free water.

3.5 LF-NMR analysis of chitosan nanoparticles dried by microwave power densities

The continuous T_2 distribution curves of UA-loaded chitosan nanoparticles during drying process at different microwave power densities are shown in Figure 5. The chitosan nanoparticles were dried by MFD at different microwave power densities, and the moisture state change showed a similar tendency. Figure 5 shows that as the MFD process continue, there is a significant decrease in the peak amplitude. The T_2 distribution tended to move to the left side as a whole in Figure 5, indicating that water mobility of chitosan nanoparticles decreased. Figure 5 shows that the similar T_2 distribution of wet chitosan nanoparticles are present at the initial stage of MFD under different microwave power densities, and the free water is firstly removed and the greater the microwave power density, the faster the free water is removed. The moisture of chitosan nanoparticles changed in the later stage of drying, and the remaining water mainly existed in the form of bound and immobile

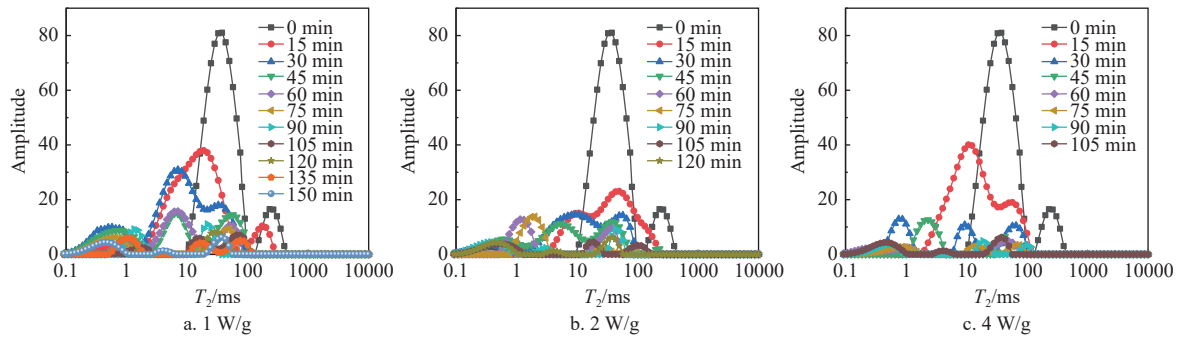

Figure 5 T_2 distributions of UA-loaded chitosan nanoparticles at different microwave power densities

water. The results were in agreement with the spray drying characteristics of saffron bioactive components encapsulation. Figure 5 shows that a higher microwave power density could better promote the conversion of water from a high degree of freedom to a low degree of freedom, resulting in different time to reach the equilibrium moisture content of 5%. The results showed that the degree of moisture conversion was different due to the different microwave power densities.

3.6 Effect of different microwave power densities on free moisture state

Figure 6 shows that the free water peak area A_{23} variation curves of UA-loaded chitosan nanoparticles at different microwave power densities. It can be seen from Figure 6 that free water peak area A_{23} gradually decreases as the drying process progresses and the greater the microwave power density, the shorter the drying time for A_{23} to reach the minimum value, indicating that the microwave is beneficial to the sublimation of moisture during the drying process. The order of free water removal under different microwave power densities is 4 W/g > 2 W/g > 1 W/g. The change trend of the free water peak area A_{23} in chitosan nanoparticles is similar to the drying curve in Figure 1a, and the change of free water content during the drying process would directly affect the drying effect.

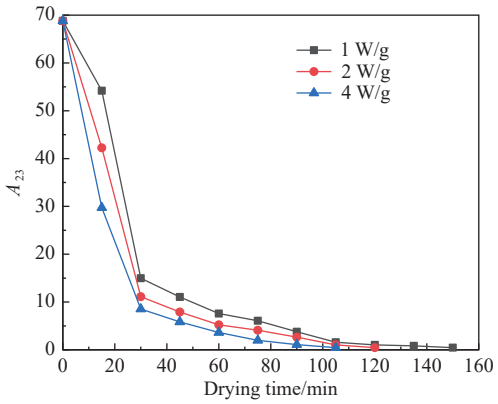

Figure 6 The free water A_{23} variation curves of UA-loaded chitosan nanoparticles during drying process at different microwave power densities

3.7 Effect of different microwave power densities on immobile moisture state

The immobile water A_{22} variation curves of UA-loaded chitosan nanoparticles at different microwave power densities are shown in Figure 7. As shown in Figure 7, the immobile water curve in the chitosan nanoparticles presented a decrease and increase alternately as the drying process progresses at 1, 2, 4 W/g. The reason for the decrease may be attributed to that a part of the immobile water migrated to the free water and then was removed after free water was removed in the early drying stage. The second reason for the reduction may lie in that the hydrophilic group structure of polysaccharides can reduce the dynamic water flowing around them, leading in the migration of immobile water to bound water[35]. The immobile water increase may be caused by that part of the unstable bound water was irradiated by microwaves and migrated to the immobile water. In addition, with the extension of the drying time, the shrinkage of chitosan nanoparticles occurred, and the concentration difference caused part of free water to migrate to immobile water[36]. The results showed that with the increase of microwave power density during the drying process of UA-loaded chitosan nanoparticles, the degree of mutual migration and transformation of water in different states increased.

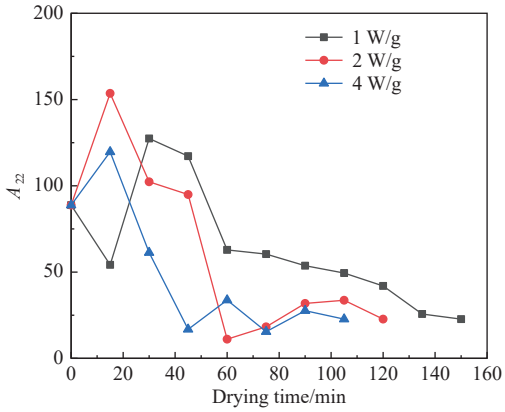

Figure 7 The immobile water A_{22} variation curves of UA nanoparticles during drying process at different microwave power densities

3.8 Effect of different microwave power densities on bound moisture state

The effect of different microwave power densities on the migration change of bound water A_{21} is shown in Figure 8. As shown in Figure 8, the bound water of UA-loaded chitosan nanoparticles during drying process displayed an increase in the whole stage followed by a decrease at different microwave power densities. At the primary stage of drying, part of the free water was combined with chitosan material, resulting in an increase in the bound water peak area A_{21}. In the later stage of drying, part of bound water is converted into immobile water and removed. The result was consistent with the change trend of Pleurotus eryngii bound water A_{21} during microwave hot-air flow rolling drying[37].

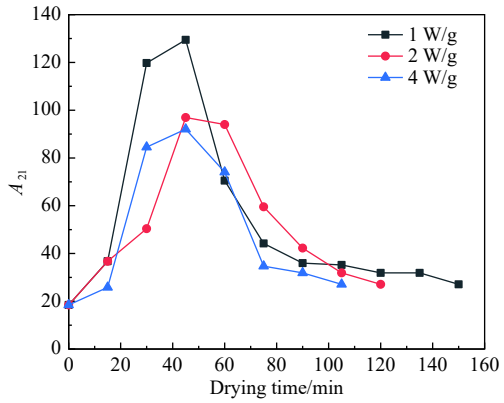

Figure 8 The bound water A_{21} variation curves of UA nanoparticles during drying process at different microwave power densities

4 Conclusions

In this study, the MFD drying process was described by drying curves, the Page model, and the LF-NMR technology was used to characterize the water distribution and changes of UA nanoparticles. The drying curves of UA-loaded chitosan nanoparticles showed a decline trend during the drying process at different microwave power density, and higher microwave power can realize shorter time to reach equilibrium moisture. The MFD process of UA-loaded chitosan nanoparticles could best be fitted by Page model. During drying process, T_2 distribution tended to move to the left side. Free water was removed at the initial stage of drying, and the remaining water mainly existed in the form of bound and immobile water in the later stage of drying. During the MFD process of chitosan nanoparticles, free water kept decreasing, the immobile water peak

area curve showed fluctuating, and the bound water peak area curve showed an increase followed by a decrease. All these findings proved the changes in the moisture content and distribution of chitosan nanoparticles during the MFD process. This study can provide a reference for exactly stimulating and optimizing MFD process of UA nanoparticles.

Acknowledgements

This work was financially supported by the National Natural Science Foundation of China under the contract of (Grant No. 32172352) and the leading talents of science and technology in the Central Plain of China (Grant No. 234200510020).

[References]

[1] Caligiani A, Malavasi G, Palla G, Marseglia A, Tognolini M, Bruni R. A simple GC–MS method for the screening of betulinic, corosolic, maslinic, oleanolic and ursolic acid contents in commercial botanicals used as food supplement ingredients. Food Chemistry, 2013; 136(2): 735–741. doi: 10. 1016/j.foodchem. 2012.08.011.

[2] Cargnin S T, Gnoatto S B. Ursolic acid from apple pomace and traditional plants: A valuable triterpenoid with functional properties. Food Chemistry, 2017; 220: 477–489.

[3] Lei Y, Sun Z, Zu Y, Zhao C, Sun X, Zhang Z, Lin Z. Physicochemical properties and oral bioavailability of ursolic acid nanoparticles using supercritical anti-solvent (SAS) process. Food Chemistry, 2012; 132(1): 319–325.

[4] Duan L L, Duan X, Ren G Y. Evolution of pore structure during microwave freeze-drying of Chinese yam. Int J Agric & Biol Eng, 2018; 11(6): 208–212.

[5] Yang Y H, Li X Z, Sheng Z. Preparation methods and release kinetics of Litsea cubeba essential oil microcapsules. RSC Advances, 2018; 8(52): 29980–29987.

[6] Zbek Z A, Ergnül P G. Optimisation of wall material composition of freeze–dried pumpkin seed oil microcapsules: Interaction effects of whey protein, maltodextrin, and gum Arabic by D-optimal mixture design approach. Food Hydrocolloids, 2020; 107: 1–13.

[7] Duan X, Yang X T, Ren G Y, Pang Y Q, Liu L L, Liu Y H. Technical aspects in freeze-drying of foods. 2016; 34(11): 1271-1285. doi: 10. 1080/07373937.2015. 1099545.

[8] Duan X, Zhang M, Li L L, Mujumdar A S. Microwave freeze drying of sea cucumber coated with nanoscale silver. Drying Technology, 2008; 26(4): 413–419.

[9] Jiang H, Zhang M, Mujumdar A S, Lim R X. Analysis of Temperature distribution and SEM images of microwave freeze drying banana chips. Food & Bioprocess Technology, 2013; 6(5): 1144–1152.

[10] Duan X, Liu W C, Ren G Y, Liu L L, Liu Y H. Browning behavior of button mushrooms during microwave freeze-drying. Drying technology:An International Journal, 2016; 34(9-12): 1373–1379.

[11] Wang R, Zhang R, Mujumdar R S. Effects of vacuum and microwave freeze drying on microstructure and quality of potato slices. Journal of Food Engineering, 2010; 101(2): 131–139.

[12] Dai J W, Xiao H W, Zhang L H, Chu M Y, Qin W, Wu Z J, et al. Drying characteristics and modeling of apple slices during microwave intermittent drying. Journal of Food Process Engineering, 2019; 42(6): 1–10.

[13] Deepak K, Ayon T, Yogesh K, Prarabdh C B. Intelligent modeling and detailed analysis of drying, hydration, thermal, and spectral characteristics for convective drying of chicken breast slices. Journal of Food Process Engineering, 2019; 42(5): 1–14.

[14] Li T S, Sulaiman R, Rukayadi Y, Ramli S. Effect of gum Arabic concentrations on foam properties, drying kinetics and physicochemical properties of foam mat drying of cantaloupe. Food Hydrocolloids, 2020; 116(6): 106492. doi: 10.1016/j. foodhyd.2020.106492

[15] Parveen K, Khatkar B S. Nutritional composition and drying kinetics of aonla fruits. Journal of Food Science & Technology, 2018; 55(8): 3135–3143.

[16] Kadriye E, Gülşah Ç, Safiye N D. Determination of the drying and rehydration kinetics of freeze dried kiwi (*Actinidia deliciosa*) slices. Heat and Mass Transfer, 2016; 52(12): 2697–2705.

[17] Yang H W, Ji J W, Wang C, Zhang L Y, Wang X D, Song P, et al. Micro-nondestructive detection of the moisture and ion of rice seeds during germination under salt stress. Int J Agric & Biol Eng, 2019; 12(2): 103–110.

[18] Song P, Kim G, Song P, et al. Rapid and non-destructive detection method for water status and water distribution of rice seeds with different vigor. Int J Agric & Biol Eng, 2021; 14(2): 231–238.

[19] Li M, Chen Y, Geng Y L, Liu F, Guo L P, Wang X. Convenient use of low field nuclear magnetic resonance to determine the drying kinetics and predict the quality properties of mulberries dried in hot-blast air. LWT-Food Science and Technology, 2021; 137: 110402.

[20] Lin S Y, Yang S L, Li X F, Chen F, Zhang M D. Dynamics of water mobility and distribution in soybean antioxidant peptide powders monitored by LF-NMR. Food chemistry, 2016; 199: 280–286.

[21] Xu F, Jin X, Zhang L. Investigation on water status and distribution in broccoli and the effects of drying on water status using NMR and MRI methods. Food Research International, 2017; 96: 191.

[22] Long C, Tian Y, Tong Q, Zhang Z, Jin Z. Effect of pullulan on the water distribution, microstructure and textural properties of rice starch gels during cold storage. Food Chemistry, 2016; 214: 702–709. doi: 10.1016/ j.foodchem.2016.07. 122.

[23] Yan J, Guan Z Y, Zhu W F, Zhong L Y, Huang X. Preparation of puerarin chitosan oral nanoparticles by ionic gelation method and its related kinetics. Pharmaceutics, 2020; 12(3). doi: 10.3390/pharmaceutics12030216.

[24] Duan X, Liu W C, Ren G Y, Ren G Y, Yang T X. Effects of different drying methods on the physical characteristics and flavor of dried hawthorns (*Crataegus* spp.). Drying Technology, 2017; 35(11): 1412–1421. doi: 10.1080/07373937. 2017.1325898.

[25] Pang Y Q, Duan X, Ren G Y, Liu W. Comparative study on different drying methods of fish oil microcapsules. Journal of Food Quality, 2017; 2017: 1–7.

[26] Wang H, Duan X, Duan L L, Ren G Y. Mutual transformation of the water binding state and moisture diffusion characteristics of Chinese yams during microwave freeze drying. Drying Technology, 2019; 1–11. doi: 10.1080/ 07373 937.2019.1693400.

[27] Martins M G, Martins D, Pena R. Drying kinetics and hygroscopic behavior of pirarucu (Arapaima gigas) fillet with different salt contents. LWT - Food Science and Technology, 2015; 62(1): 144–151.

[28] Beigi M. Mathematical modelling and determination of mass transfer characteristics of celeriac slices under vacuum drying. Periodica Polytechnica Chemical Engineering, 2016; 61. doi: 10.3311/PPch.9271.

[29] Li M, Chen Y N, Wang X, Cheng S P, Liu F, Huang L Q. Determination of drying kinetics and quality changes of *Panax quinquefolium* L. dried in hot-blast air. LWT - Food Science and Technology, 116, 108563-108563. doi: 10.1016/j.lwt. 2019.108563.

[30] Martín-Gómez J, Varo M N, Mérida J, Serratosa M P. Influence of drying processes on anthocyanin profiles, total phenolic compounds and antioxidant activities of blueberry (*Vaccinium corymbosum*). LWT - Food Science and Technology, 2020; 120. doi: 10.1016/j.lwt.2019.108931.

[31] Duan L, Xu D, Ren G. Water Diffusion Characteristics and Microwave Vacuum Freeze-Drying Modelling of Chinese Yam (*Dioscorea opposite*) Tubers. Food Science, 2019; 40(1): 23–30.

[32] Sehrawat R, Nema P K, Kaur B P. Quality evaluation and drying characteristics of mango cubes dried using low-pressure superheated steam, vacuum and hot air drying methods. LWT - Food Science and Technology, 2018; 92: 548–555.

[33] Wang C, Wang X, Liu C Y, Liu C H. Application of LF-NMR to the characterization of camellia oil-loaded pickering emulsion fabricated by soy protein isolate. Food Hydrocolloids, 2021; 112: 106329.

[34] Wang R, Li M, Wei Y, Guo B L, Brennan M, Brennan C S. Quality differences between fresh and dried buckwheat noodles associated with water status and inner structure. Foods, 2021; 10(1): 187.

[35] Einhorn-Stoll U, Hatakeyama H, Hatakeyama T. Influence of pectin modification on water binding properties. Food Hydrocolloids, 2012; 27(2): 494–502.

[36] Cheng S, Li R R, Yang H, Wang S Q, Tan M Q. Water status and distribution in shiitake mushroom and the effects of drying on water dynamics assessed by LF-NMR and MRI. Drying Technology, 2020; 38(8): 1001–1010.

[37] Su D B, Lv W Q, Wang Y, Li D, Wang L J. Drying characteristics and water dynamics during microwave hot-air flow rolling drying of *Pleurotus eryngii*. Drying Technology, 2019; 1–12. doi: 10.1080/07373937.2019. 1648291.